AGU PUBLICATIONS

Water Resources Research

RESEARCH ARTICLE
10.1002/2013WR014580

Key Points:
- The same volume of runoff can generate different total sediment yields (~200%)
- Erosion enhancement or impediment effects exerted by the shielding layer
- Two time scales and three characteristic regimes

Supporting Information:
- Supplement readme
- Table S1
- Figure S1, S2, S3

Correspondence to:
J. Kim,
kjongho@umich.edu

Citation:
Kim, J., and V. Y. Ivanov (2014), On the nonuniqueness of sediment yield at the catchment scale: The effects of soil antecedent conditions and surface shield, *Water Resour. Res.*, *50*, 1025–1045, doi:10.1002/2013WR014580.

Received 13 AUG 2013
Accepted 13 JAN 2014
Accepted article online 17 JAN 2014
Published online 6 FEB 2014

On the nonuniqueness of sediment yield at the catchment scale: The effects of soil antecedent conditions and surface shield

Jongho Kim[1] and Valeriy Y. Ivanov[1]

[1]Department of Civil and Environmental Engineering, University of Michigan, Ann Arbor, Michigan, USA

Abstract The understanding of reasons leading to nonuniqueness of soil erosion susceptibility is still inadequate, yet indispensable for establishing general relations between runoff volume and sediment yield. To obtain relevant insights, we performed a series of numerical simulations with a detailed hydrodynamic model using synthetic storms of varying intensity, duration, and lag time between events as representations of different hydrologic response conditions in a zero-order catchment. The design targeted to generate surface flow and "perturb" soil substrate by a first rainfall event, creating a set of initial conditions in terms of flow and deposited sediment prior to the onset of a subsequent rainfall event. Due to the differential effect of (re)detachment and (re)entrainment processes on soil particles of varying sizes, the deposited sediment mass formed shielding layer. One of the essential results is that unless the initial condition of flow and sediment is identical, the same volume of runoff can generate different total sediment yields and their variation can reach up to ~200%. The effect is attributed to two major conflicting effects exerted by the deposited "initialization" (soil antecedent condition) sediment mass: erosion enhancement, because of supply of highly erodible sediment, and erosion impediment, because of constrain on the availability of lighter particles by heavier sediment. Consistently with this inference, long-term simulations with continuous rainfall show that a peculiar feature of sediment yield series is the existence of maximum before the steady state is reached. The two characteristic time scales, the time to peak and the time to steady state, separate three characteristic periods that correspond to flow-limited, source-limited, and steady-state regimes. These time scales are log linearly and negatively related to the spatially averaged Shields parameter: the smaller the rainfall input and the heavier a given particle is, the larger the two scales are. The results provide insights on how the existence of shield operates on erosion processes, possibly implying that accurate short-term predictions of geomorphic events from headwater areas may never become a tractable problem: the latter would require a detailed spatial characterization of particle size distribution prior to precipitation events.

1. Introduction

Estimation of sediment yield (*SY*) at the catchment scale plays a significant role for optimal design of hydraulic structures, such as bridges, culverts, reservoirs, canals, harbors, and detention basins, as well as making informed decisions in environmental and ecological management. The *SY* is defined here as the total sediment mass discharged by a basin at an outlet section over a duration of a hydrologic event. Prior experimental studies focused on obtaining flow and sediment data in a search of unique relationships between runoff (specifically, volume and peak) and characteristics of basin sediment yield [*Pierson et al*., 2001; *Harmel et al*., 2006; *Nearing et al*., 2007]. These relationships have been used to predict sediment yield from flow information due to the relatively high difficulties in measuring sediment. Generally, sediment yield is assumed to increase with flow volume (*FV*) for a given basin area [*Nearing et al*., 2007; *Pierson et al*., 2001]. Yet there are substantial nonlinearities in the basin response that can trigger remarkable variations in any derived unique *SY-FV* relationship, thus making the estimation of *SY* very uncertain. Indeed, the actual event-scale sediment yield produced by a river basin can vary significantly for the same metric of hydrologic response (see e.g., *Nearing et al*. [2007, Figure 2] reporting data from watersheds in the U.S. Southwest).

Such nonuniqueness of sediment yield is common for many locations around the world and can be attributed to nonlinearities associated with several possible contributing factors. (1) Given the same rainfall,

sediment output at a basin outlet is nonlinear with respect to the size of a watershed. Drainage basins of higher orders have lower delivery ratios (defined as the ratio between *SY* and the total eroded material), as compared to smaller watersheds, due to larger watershed storage capacity in the floodplain [*Lane et al*., 1997; *Phillips*, 2003]. (2) Sediment dynamics strongly depend on land use, land cover, and conservation management practices [*Harmel et al*., 2007; *Ward et al*., 2009; *Notebaerta et al*., 2011; *Defersha and Melesse*, 2012]. As an example, for two major cropping systems in Texas Blackland Prairies, annual soil loss in regions producing small grain (wheat or oat) is significantly lower than that of areas with row crop production (corn or sorghum) [*Harmel et al*., 2006]. In watersheds with either shrub or grass vegetative cover in southeastern Arizona, the mean soil loss in shrubby areas is higher than that in grassy sites [*Nearing et al*., 2005]. (3) Erosion is higher at sites with steeper and longer slopes [*Defersha et al*., 2011]. This effect is particularly pronounced in regions where gravity plays a significant role in sediment release and movement. However, the relationship between site slope and sediment yield is subject to substantial variations in areas of mild topography, where the processes related to flow characteristics (e.g., the development of narrower and faster flow threads) and flow patterns (e.g., connectivity between patches of wider or narrower flows) are predominant over the gravity-controlled processes [*Armstrong et al*., 2011]. (4) Precipitation characteristics (intensity, frequency, duration, and volume) substantially affect the variability of sediment yield. Only several extreme storms can be responsible for most of the total erosion loss over a long period [*Edwards and Owens*, 1991; *Nearing et al*., 2007]. The sequence of rainfall events may also impact the amount of the total erosion [*Romkens et al*., 2001]. (5) Surface conditions such as soil moisture content, crust formation, sealing, slaking, and organic matter contents can appreciably influence runoff and erosion generating processes [*Le Bissonnais et al*., 1995; *Mamedov et al*., 2006; *Wuddivira et al*., 2009].

In addition to these aforementioned reasons, the type of soil and its particle-size distribution (PSD) may result in selective erosion and transport of sediment that depend on a grain size and the corresponding settling velocity [*Rose et al*., 1983b, 1983a; *Hairsine and Rose*, 1991; *Hairsine et al*., 1999]. Specifically, smaller particles have low settling velocities and are prone to move far from their original position of detachment. Conversely, larger particles can settle quickly near their source locations because of their heavier immersed weight [*Sander et al*., 1996]. Larger particles can also form a shield on soil bed and protect underlying material from rainfall detachment and runoff entrainment [*Kinnell*, 1993; *Hairsine et al*., 1999]. Experimental research on the formation and temporal development of a shielding layer has demonstrated a range of relevant phenomena [*Heilig et al*., 2001; *Walker et al*., 2007; *Armstrong et al*., 2012]. Specifically, *Heilig et al*. [2001] first confirmed the existence of a shielding layer through a simple experimental design under rainfall-induced erosion. *Walker et al*. [2007] examined the role of infiltration on soil erosion, and argued that increased infiltration makes the formation of a shielding layer more rapid by increasing the vertical deposition rate. *Armstrong et al*. [2012] further investigated the effects of slope, ponding depth, and infiltration. The first two variables were found to be significant factors controlling shield development, while the effects of infiltration were minor. All of these experimental studies corroborated the formation of a shielding layer through photographs, video image processing, or statistical analyses and presented the implications of several parameters on the process. The studies primarily focused on relatively simple, small-scale experiments over a short term (hourly time scales) by using plot-scale domains: a small horizontal soil surface ($7 \times 7 \times 7$ cm^3) [*Heilig et al*., 2001], a soil chamber with a diameter of 7.5 cm [*Walker et al*., 2007], and Perspex soil boxes ($25 \times 25 \times 15$ cm^3) [*Armstrong et al*., 2012].

At a laboratory scale of an experimental study, the development of a shielding layer was investigated with respect to the boundary effects of flume lateral width [*Jomaa et al*., 2010] and protection by large-scale elements within a channel [*Jomaa et al*., 2012; *Kim et al*., 2012a; *Jomaa et al*., 2013]. Further, the impacts of antecedent and initial soil conditions on variability of *SY* were described through an experiment in which several successive rainfall events were considered for a small-scale ($1\ \text{m} \times 6\ \text{m}$) flume [*Jomaa et al*., 2013]. Since technical challenges prevented direct, continuous monitoring of flow/sediment variables at flume internal points, the observations were presented mainly at the outlet. An explicit observation of the evolution of spatially and temporally varying shielding layer was not reported.

Several modeling studies [*Kinnell*, 2006, 2009, 2012] have illustrated the development of surface shield based on results of a numerical model applied to a planar domain. They emphasized that the rate at which particles move across the surface and the distance over which the movement takes place are the key factors in forming a surface shield. The parameterization used in these studies had a mechanistic basis, given

undeveloped, shallow flow conditions. The studies of Kinnel [*Kinnell*, 2005, 2006, 2009, 2012] followed a "Lagrangian" approach: given a size distribution, the sediment discharge was determined by tracking the pathline of each particle and investigating the distance and travel time of the motion. While this manner of representing the dynamics offers certain flexibility in terms of understanding the details of fluid and sediment behaviors, it also includes a number of parameterization challenges that are difficult to overcome using data obtained with well-established methodologies.

Several additional numerical studies further demonstrated variability in soil erosion as a result of process interactions during armoring sand weathering [*Sharmeen and Willgoose*, 2006; *Willgoose and Sharmeen*, 2006; *Cohen et al*., 2009, 2010, 2013]. They were carried out through a representation of two conflicting effects on soil erosion: erosion growth (mostly) or decrease due to weathering interactions (in some cases) and armoring effects of coarser materials [*Sharmeen and Willgoose*, 2006]. Due to the high fraction of rock fragments, significant armoring effects were demonstrated for a noncohesive sandy gravel soil [*Sharmeen and Willgoose*, 2007]. Although these studies could capture the phenomena associated with coarsening of surface materials and weathering effects, these numerical experiments focused on simulations over the long term, usually more than 100 years [*Sharmeen and Willgoose*, 2006, 2007; *Cohen et al*., 2009, 2010, 2013]. Such time scales required additional simplifications such as parameterizations of flow complexity (depth and velocities) to be explained by the Manning equation, and sediment fluxes considered through a simple empirical equation.

At larger spatial scales, e.g., watershed with complex topography, and over the long term, none of the aforementioned studies addressed the effects of relevant variables on the formation and decay of a shielding layer and its impact on the erosion process and basin sediment loss. The primary goal of this study is to obtain mechanistic insights on why size-selective erosion processes can result in nonunique sediment yield for the same runoff volume by exploring internal dynamics of a watershed system. The specific objectives are (1) to investigate the effects of rainfall patterns on sediment yield, (2) to elucidate the occurrence of unsteady phenomena in the process of erosion, given a steady-state hydraulic flow condition, and (3) to describe unsteady patterns and attribute them to critical time scales in the dynamics of morphologic variables. The study is based on a numerical investigation of sediment yield response from a zero-order watershed (the total area is 14×28 m^2) forced by a set of synthetic rainfall events. The modeling scenarios are constructed such that perturbations caused by prior rainfall impacts the initial condition for a succeeding storm event in terms of either (i) flow (smaller/larger depth) or soil bed (intact/loose). The various initial conditions lead to the nonuniqueness of basin sediment yield with respect to the same runoff. The numerical model used in this study is the two-dimensional Hairsine-Rose erosion/sediment transport model coupled to a fully distributed hydrology and hydrodynamic model.

2. Model Description and Simulation Design

2.1. Numerical Model: tRIBS-FEaST

The basic premise of this study is that soil bed with multiple particle sizes can form a shield by relatively larger particles, which can lead to a nonunique sediment response with respect to the same forcing. The appropriate formulation of erosion and sediment transport model capable of incorporating features required for a numerical exploration of the above assertion is the Hairsine-Rose (H-R) model [*Hairsine and Rose*, 1991, 1992; *Sander et al*., 2007a]. It represents a mechanistic erosion and sediment transport model that can describe the formation and development of surface shield. Since the original research in 1990s, a significant amount of research on the Hairsine-Rose formulation has confirmed its appropriateness; it has been addressed analytically [*Sander et al*., 1996; *Hairsine et al*., 1999; *Hairsine et al*., 2002; *Sander et al*., 2002; *Hogarth et al*., 2004b], numerically [*Hogarth et al*., 2004a; *Heng et al*., 2009; *Kim et al*., 2013], and experimentally [*Proffitt et al*., 1991; *Heilig et al*., 2001; *Rose et al*., 2007; *Walker et al*., 2007; *Armstrong et al*., 2011; *Heng et al*., 2011; *Armstrong et al*., 2012]. Further, these unsteady, two-dimensional, advection-dominated sediment transport equations have been successfully combined with flow mass and momentum equations, such as the Saint-Venant equations [*Leendertse*, 1967; *Liggett*, 1968; *Abbott*, 1974] using the Finite Volume framework [*Heng et al*., 2009; *Papanicolaou et al*., 2010; *Kim et al*., 2013]. In a latest effort, a quasi three-dimensional watershed scale hydrology model that addresses the problem of partitioning of water and energy budgets has been coupled to the system of flow and sediment equations on an unstructured

triangular grid [*Kim et al*., 2012b, 2013]; it is called the tRIBS-FEaST: TIN (Triangulated Irregular Network)-Based Real Time Integrated Basin Simulator (tRIBS) [*Ivanov et al*., 2004] and Flow, Erosion and Sediment Transport (FEaST). The formulation adopts the "Eulerian" approach: at a given point in space and time, the H-R formulation considers uplift and fall of each particle size and computes its concentration and deposition after the volume of water containing the sediment moves downstream at the advection flow velocity. The two-dimensional description of flow motions caused by variations in topography and meteorological forcing, as well as hydrologic partition related to vegetation cover, landuse, and subsurface processes are explicitly captured. For a more detailed description, the reader is referred to *Kim et al*. [2012b] and *Kim et al*. [2013].

2.2. Modeling Erosion Processes in a Zero-Order Catchment

A zero-order basin that exhibits both hillslope and flow convergent areas is selected for a numerical analysis in this study because it includes more complex, "realistic" topography, as compared to planar domains used in most experimental studies. The basin dynamics can include the processes of both rainfall-induced detachment and runoff-driven entrainment. The former type of erosion process is generally predominant in headwater areas of the basin, while the latter in the flow convergent, channel areas. These dynamics are therefore representative of mechanisms operating in real catchments exhibiting a range of slopes. The relatively small size of the basin permits computational feasibility. Another reason for the choice of the study domain is the necessity to exclude the effects of fluvial processes occurring in perennial channels of higher-order catchments, where substantial flow depths influence the process of rainfall (re)detachment [*Laws and Parsons*, 1943; *Mutchler and McGregor*, 1983; *Proffitt et al*., 1991], or the effects of other mechanisms such as turbulent characteristics of flow, the diffusion process of sediment motion, and vertical variations of the water flow velocity may become dominant.

Soil erosion and sediment transport are very complex phenomena and all relevant processes are extremely difficult to describe at a high detail in a numerical model. Before the numerical results of simulations are presented, one needs to address strengths and weaknesses of the employed modeling approach. The advantages of the employed model are as follows. First, the two-dimensional flow motions caused by topographic variations in the zero-order catchment or obstacles can be well computed in a spatiotemporally manner [*Kim et al*., 2012a]. The model can calculate all primary variables such as flow depths, velocities, concentrations, deposited masses, and elevation changes in a dynamic or nonsteady fashion. One of the derivative variables, the shielding factor H is also computed and updated each time step. In contrast to previous modeling studies, no assumptions are needed to represent the dynamic evolution of the deposited layer: the factor H is dynamically computed and updated each time step of the hydrodynamic model as a result of the local balance of processes of redetachment, reentrainment, and deposition, also implicitly affected by the processes of detachment and entrainment in advection-dominated sediment transport [see *Kim et al*., 2013 for details]. Next, the Hairsine-Rose formulation can render the phenomena of detachment, deposition, and sediment transport in a more physically consistent fashion [*Sander et al*., 2007b], as compared to numerical models using the transport capacity concept, such as KINEROS [*Woolhiser et al*., 1990], WEPP [*Nearing et al*., 1989], and tRIBS-Erosion [*Francipane et al*., 2012]. The latter models employ two different erosion source equations depending on whether the flow conditions are under net eroding or net depositional regimes and therefore, under a given flow condition, only a single erosional regime can occur. However, empirical evidence on detachment and deposition processes testifies that each process occurs simultaneously and continuously. *Polyakov and Nearing* [2003] pointed out that models based on a single, prescribed transport capacity fail to simulate soil conditions with multiple particle sizes and evolving composition of the bed, because the transport capacity is not unique during simulations in such conditions [*Polyakov and Nearing*, 2003; *Sander et al*., 2007b]. The coupled model adopting the Hairsine-Rose formulation can satisfactorily resolve such challenging effects caused by both preferential deposition in a water column and a physical protection by the deposited layer.

In contrast, there is a set of processes that are not or cannot be fully addressed by the formulation used in this study. (1) The erosion phenomena related to subsurface water content and the effect of negative or positive soil matric pore pressures are not considered [*Simon and Collison*, 2001]. For instance, as soil becomes saturated, erosion can increase due to the growth of pore water pressure that reduces soil cohesive strength [*Simon and Collison*, 2001]. (2) Erosion enhancement due to increasing aggregate breakdown and slaking, which is attributed to air burst within pores of aggregates during rapid wetting [*Le Bissonnais*

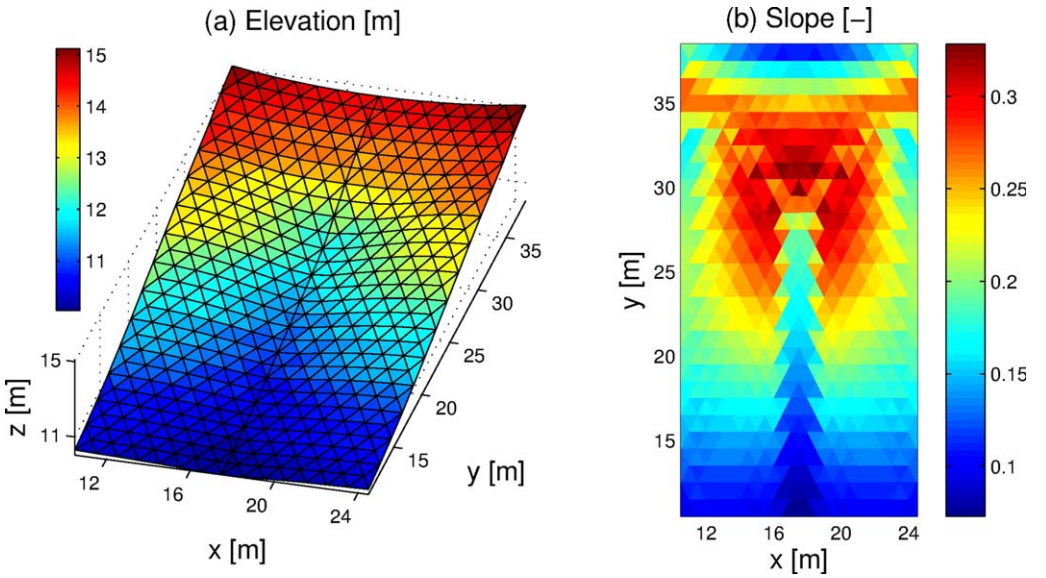

Figure 1. Illustrations of (a) elevation and (b) slope fields of the simulation domain.

et al., 1989; *Rudolph et al*., 1997]. The process of slaking is more pronounced in soils where organic matter contributing to binding forces among mineral particles is low. (3) Repelling of soil particles in condition of wet soil. This process is due to an interaction between a layer of positive charges composed of chemical cations (e.g., sodium, calcium, and magnesium) surrounding clayey soil particles that carry negative electrical charge. (4) Drying of slaked clayey soil that leads to crusting and sealing and may result in a reduction of infiltration and growth of runoff and erosion [*Le Bissonnais et al*., 1989]. (5) The employed model cannot represent "subgrid" processes, such as a flow motion occurring in narrower, faster flow threads of the assumed planar surface of a computational cell (i.e., a triangle). Specifically, the numerical model does not require a "rill" or a "stream parameterization," provided the resolution of computational cells is small enough to capture the scale and the actual representation of a rill or a stream. If the resolution is coarser, however, the model formulation assumes sheet flow within a cell. In summary, all of the above processes related to a degree of soil saturation, slaking by trapped air, repelling between chemical cations (dispersion), crusting, and rill formation are excluded in this study. The significance of this assumption is difficult to assess as better parameterizations or exact mathematical theories associated with these processes are needed for a more complete numerical treatment of the erosion process. However, given that the skill of the Hairsine-Rose formulation with conventionally defined sink and source terms has been confirmed in earlier studies using similar space-time scales, the appropriateness of Hairsine-Rose approach for this study appears to be fully justified [*Heng et al*., 2011].

2.3. Simulation Setup

2.3.1. Domain and Modeling Configuration

Sediment yield at an outlet of a zero-order catchment [*Ivanov et al*., 2010] is simulated for different precipitation patterns. The domain is 14 m wide and 28 m long and is resolved with a triangular mesh of about 1 m spacing. Local slopes range from 7.3 to 32.8% (see Figure 1). Such a relatively small catchment, as compared to most instrumented, real-world watersheds, is nonetheless significantly larger than domains used in experimental studies exploring size-selective erosion processes. The number of mesh nodes and triangular cells are 435 and 812 (Figure 1). The time step used for runoff generation routine is 7.5 min. The time step used for the simulation of flow hydrodynamics and erosion-transport modeling components is 0.2 s. For the entire range of simulation scenarios, the initial conditions for flow and soil bed state are specified as intact and dry bed conditions, i.e., no flow and no loose, detached materials. The specified boundary conditions are a solid slip wall condition for all boundaries except for outlets, and the free outflow boundary condition for outlet cells. *Kim et al*. [2013] provides all relevant details.

Table 1. A Summary of Five Principal Simulation Cases[a]

Name	Number of Events	Number of Subcases	Duration, T_r (h)	Intensity RI (mm/h)	Lag Time T_b (h)
Case 1	2	35	$T_{r,1} = T_{r,2} = 1$	$RI_1 = RI_2 = 10, 30, 50, 70, 90$	0, 2, 4, 6, 8, 10, 12
Case 2	2	25	$T_{r,1} = T_{r,2} = 1$	$RI_1 \neq RI_2 = 10, 30, 50, 70, 90$	12
Case 3	2	25	$T_{r,1} = T_{r,2} = 1$	$RI_1 \neq RI_2 = 10, 30, 50, 70, 90$	0
Case 4	1	5	$T_{r,1} = 15, 7.5, 5, 3.75, 3$	$RI_1 = 20, 40, 60, 80, 100$	
Case 5	1	5	$T_{r,1} = 1440$	$RI_1 = 10, 30, 50, 70, 90$	

[a]The total number of simulations is 95.

2.3.2. Rainfall *Forcing*

Five synthetic simulation cases with different rainfall patterns are designed (see Table 1 and Figure 2). The generated rainfall forcing for the domain is spatially uniform, while temporally variable and defined by the rainfall intensity (RI), duration (T_r), and lag time between events (T_b). The first case of forcing (Case 1) represents a composition of two rectangular "pulses" of rainfall (E_1 and E_2), both of which have the same intensity and duration of 1 h ($RI_1 = RI_2$, $T_{r,1} = T_{r,2} = 1$). Variables that are varied in Case 1 are the magnitude of rainfall intensity (RI) and the lag time between the two events (T_b). As a result of permutation of five rainfall intensities ($RI_1 = RI_2 = 10$, 30, 50, 70, and 90 mm/h) and seven lag times ($T_b = 0$, 2, 4, 6, 8, 10, and 12 h), Case 1 includes 35 subcases. The varying lag times between the two rainfall pulses imply different initial states of overland flow within the domain for the second rainfall event.

In the second and third rainfall forcing cases (Cases 2 and 3), two rainfall pulses are also used. They have the same duration of 1 h but may have different rainfall intensities ($RI_1 \neq RI_2$, $T_{r,1} = T_{r,2} = 1$). Both cases consist of 25 subcases that correspond to permutations of five rainfall intensities for the first event ($RI_1 = 10$, 30, 50, 70, and 90 mm/h) and for the second event ($RI_2 = 10$, 30, 50, 70, and 90 mm/h). The only difference between Cases 2 and 3 is the time lag between the two pulses: $T_b = 12$ h for Case 2 and $T_b = 0$ for Case 3. The reason for the chosen T_b set to 12 h (Case 2) is because this time period was determined to be sufficiently long to exclude the effects of overland flow initialization for the second event; different rainfall intensities during the first rainfall pulse target the generation of different initial conditions of soil bed for the subsequent event. In contrast, Case 3 uses $T_b = 0$, which generates different initial conditions in terms of both flow and sediment for the second simulation event.

The Case 4 corresponds to five different scenarios with a single rainfall event such that the total precipitation depth of 300 mm is imposed. The rainfall intensities, $RI_1 = 20$, 40, 60, 80, and 100 mm/h, therefore define the rainfall duration ($T_{r,1}$): 15.0, 7.5, 5.0, 3.75, and 3.0 h, respectively. The Case 4 is useful for identifying how rainfall events of the same volume but different intensities affect sediment erosion.

The last set of rainfall forcing scenarios (Case 5) is designed to have a single rainfall event that has a duration of 60 days. Five rainfall intensities are used: $RI_1 = 10$, 30, 50, 70, and 90 mm/h. Such a long event duration is of course entirely hypothetical but this long-term simulation can be helpful in identifying how unsteady sediment dynamics occur and temporally transform, even though flow motion exhibits steady state throughout most of the simulation period.

2.3.3. Soil Characterization

In this study, silty sand soil that has four different particle types, each contributing an equal fraction of 25%, is considered as an initial bed condition for all simulation cases (i.e., at time equal to zero). The sediment sizes of considered soil particle types are assumed to be 0.02, 0.05, 0.1, and 0.5 mm, respectively. The smallest particle type is called S1, the second smallest and progressively larger particle types are, respectively, denoted as S2, S3, and S4. Their corresponding settling velocities, $v_{1,\ldots,4}$, are 0.000276, 0.0017, 0.0062, and 0.0619 m/s. They are calculated using a formula of *Cheng* [1997].

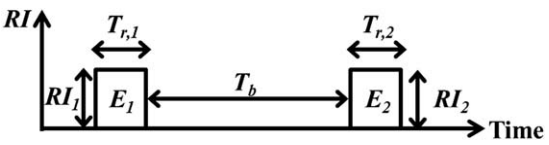

Figure 2. A schematic diagram of characteristic variables describing precipitation patterns used as forcing in this study: E denotes an event, i.e., a rectangular "pulse" of rainfall; RI is the corresponding rainfall intensity; T_r is the event duration; and T_b is the time lag between two events. The subscripts "1" and "2" refer the first and second rainfall events, respectively.

Table 2. The Model Parameters Used to Represent Hydrologic, Hydraulic, and Sediment Erosion-Transport Dynamics[a]

Parameter	Description	Value	Unit	Usage
n	Manning coefficient	0.03	$s/m^{1/3}$	Flow
a_0	Detachability of original soil	20.0	kg/m^3	Erosion
a_d	Detachability of deposited soil	2000	kg/m^3	Erosion
F	Effective fraction of excess stream power	0.01		Erosion
Ω_{cr}	Critical stream power	0.0695–0.169	W/m^2	Erosion
J	Specific energy of entrainment	750	m^2/s^2	Erosion
M_t^*	Deposited mass needed to sheild original soil	2.7	kg/m^2	Erosion
D_r	Mean raindrop size	2.0	mm	Erosion
b	An exponent in power law by *Proffitt et al.* [1991]	1.0		Erosion
K_s	Saturated hydraulic conductivity	0.0	mm/h	Soil

[a]All parameter values are time invariant.

Note that when fine-sized dry clayey soil is subjected to wetting, aggregate slaking and breakdown will occur; conversely, crust on soil is formed when slaked soil dries. Additionally, clay particles containing chemical elements (sodium, in particular) are prone to separate themselves from soil aggregates in wet conditions. Since these structural (slaking) and chemical (dispersion) mechanisms can only be implicitly incorporated in the parameters related to erodibility, fine-sized particles are excluded from the presented numerical analysis.

An impervious soil surface condition is assumed for all simulation scenarios to exclude the processes of infiltration and subsurface flow. While the latter certainly affects surface runoff generation, the aim of the study is to investigate the effects of the dynamic evolution of a shielding layer on the erosion and sediment processes in conditions of clearly identifiable precipitation patterns. The impact of runoff-generating processes is however indirectly accounted for through the imposed magnitudes of rainfall intensity.

2.3.4. Model Parameterization

Every model that involves a description of physical phenomena faces a challenge of parameter identification. Choosing proper values for these parameters is a necessary step before exploratory simulations. The parameters are usually determined either by referring to previous research described in literature or through a process of manual/automated calibration. In this synthetic study, the parameters summarized in Table 2 refer to previous research [*Heng et al*., 2011; *Francipane et al*., 2012; *Kim et al*., 2013]. The effort of calibrating the parameters of critical stream power (Ω_{cr}) is reduced through the relationship suggested by *Heng et al*. [2011] [see *Kim et al*. [2013, equation (30)]. This relationship results in the spatially varying range of 0.0695–0.169 W/m^2 for Ω_{cr}, depending on the local domain slope, when the critical Shields parameter for incipient motion is equal to 0.045.

The values of parameters J and F used in this study are different from those reported in earlier research (see a summary of parameter values in Table S1 of the supporting information). Specifically, the value of J is much higher, while that of F is smaller than what was obtained in a few physically based studies that combined flume experimentation and analytical derivations [*Proffitt et al*., 1993; *Misra and Rose*, 1995; *Rose et al*., 2007]. Using the reported range of parameter values (i.e., $J = 1.89\ m^2/s^2$ and $F = 0.1$), we attempted to calibrate the tRIBS-FEaST model for 10 erosion events in the Lucky Hills watershed [*Kim et al*., 2013], as the basin has been extensively monitored in terms of runoff and sediment yield, representing one of few real-world domains with a large set of concurrent meteorology-hydrology-sediment data. However, a satisfactory model performance in terms of sediment yield could not be obtained, despite many combinations of the parameters J and F with the other erosion parameters. This difficulty appears to be related to the issue of parameter "scale." The reported ranges of parameters J and F are certainly acceptable for controlled laboratory experimental conditions at small scale, such as those in studies of *Proffitt et al*. [1993], *Misra and Rose* [1995], and *Rose et al*. [2007]. They are however not necessarily universal and applicable to conditions of a larger watershed scale, where complex topography, unsubmerged vegetation, and rock/debris fragments modify small-scale flow conditions, leading to a nontrivial "upscaling" impact on the parameter values. Observations in this larger-scale watershed that exhibits 2-D variations of surface/flow/erosion/transport conditions indicate that a different range of upscaled parameter values is more appropriate. The specific

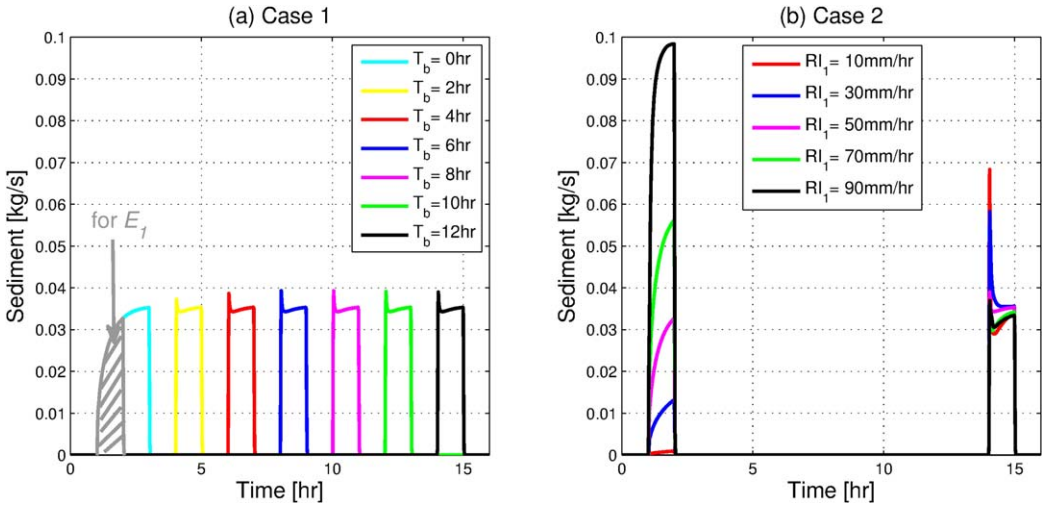

Figure 3. The simulated sedigraphs: (a) for the rainfall intensities $RI_1 = RI_2 = 50$ mm/h (Case 1; note that sedigraph corresponding to the first event is denoted with the gray line, hour 1–2); (b) for different rainfall intensities during the first rainfall event $RI_1 = 10, 30, 50, 70, 90$ and the second rainfall event with an intensity of $RI_2 = 50$ mm/h (Case 2).

values chosen for this study are taken from *Kim et al*. [2013] and further research on appropriate scaling relationships for erosion parameters is warranted.

For calibrating the deposited mass needed to shield original soil completely, we employ a single value although this represents an assumption since the value can be spatially temporally dependent on the size and velocity of raindrops and flow depth. In the calculation of the shield effect factor by water flow [see *Kim et al*. [2013, equation (9)], the mean raindrop size is assumed to be 2 mm and the exponent is assumed to be 1.0 [*Heng et al*., 2011]. Since the study essentially focuses on the movement of flow and sediment, the values of landuse and soil parameters are based from previous studies applied for the Lucky Hills watershed in southeastern Arizona, U.S.A. [*Fatichi et al*., 2012; *Francipane et al*., 2012; *Kim et al*., 2013]. The densities of sediment (ρ_s) and water (ρ_w) are 2700 and 1000 kg/m^3, respectively, and the porosity of the bed is 0.46. The Manning coefficient equal to 0.03 is chosen to represent bed roughness.

3. Simulation Results and Discussion

Simulation cases addressed in this study are designed (section 2.3.2), so that several rainfall characteristics are varied: rainfall intensity (RI), duration (T_r), and lag time between events (T_b). Different precipitation patterns are employed to investigate the effects of the frequency of rainfall events (Case 1), the arrangement and sequence of events (Cases 2 and 3), and the long-term duration of rainfall (Cases 4 and 5) on the non-uniqueness of basin sediment yield.

3.1. Temporal Characteristics of Flow and Sediment: Hydrograph and Sedigraph

While Case 1 is designed to permit different initial conditions in terms of flow depth distribution, the generated runoff flows out of the domain rapidly and the hydraulic effects of the first rainfall event on the second one are very limited. Simulated sedigraphs for the rainfall intensity of 50 mm/h are shown in Figure 3a for different values of T_b. As seen, while the sedigraphs for the first and second events are always different, the time series of sediment yield for the second event are nearly indistinguishable with respect to variations in T_b. Even for a very small lag between the two events ($\sim$15 min), the sediment rates do not change considerably (not shown). This result implies that while the initial conditions of overland flow within the domain might somewhat differ in the considered cases, they do not significantly influence the amount of sediment yield for the second rainfall event.

Figure 3b illustrates sedigraphs for the five subcases of Case 2 (among the total of 25). Specifically, five rainfall events of different magnitudes are followed by a rainfall event that has an intensity of 50 mm/h. In contrast to the previous results, the varying rainfall intensities of the first event generate different conditions of

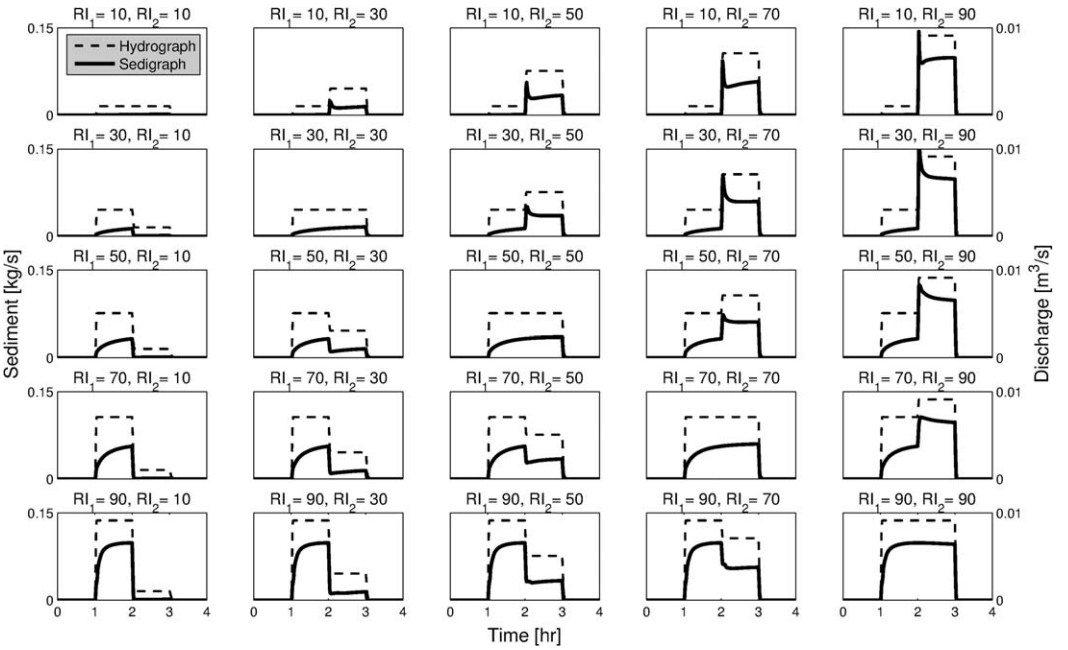

Figure 4. The simulated hydrographs and sedigraphs for Case 3. The left axis in all subplots corresponds to sedigraph series (solid line), while the right axis corresponds to hydrograph series (dashed line).

the deposited sediment layer that serves as initialization for the second event. This results in nonunique sedigraph series for the second event, in spite of the same rainfall input of 50 mm at the same intensity. The occurrence of early peak and the following convergence of sedigraphs shown in the second rainfall event were also observed in a flume study (see "E1" and "E2" in *Jomaa et al.* [2013, Figure 1]).

All simulated hydrographs and sedigraphs for the Case 3 are displayed in Figure 4. As seen, the hydrographs peak very rapidly, near the beginning of all rainfall events, implying that the times of concentration are very small. The flow remains at steady state, unless rainfall input changes. In this small impermeable domain, the flow response to a given rainfall is linear: the relationship between the rainfall input and the flow is always identical regardless of the configurations of rainfall events. However, the response of sediment to the rainfall forcing is apparently nonlinear: a notable feature is that sedigraphs may not peak within the duration of a rainfall event and may not approach the steady state. Depending on the magnitude of the first rainfall event, the second rainfall event can be highly affected. For example, for varying magnitudes of the first event and a fixed subsequent rainfall, there are considerable changes in the sediment rate series corresponding to the second event. Note that there is no change in the flow series (see any set of five column-wise subplots in Figure 4).

The simulated sedigraphs for Case 4 is shown in Figure 5a and for Case 5 in Figure 5c. The obtained sedigraphs for these fairly long-term simulations emphasize the unsteady dynamics of erosion processes. For a given rainfall intensity and duration, sediment rate quickly increases and peaks early; after that, the series exhibit a gradual decrease and an asymptotic approach to the steady state. For higher rainfall intensities, the peak of sediment rate as well as the steady state is achieved relatively faster (the associated time scales will be addressed in section 3.5).

3.2. Spatial Characterization of Flow and Sediment Dynamics

Selected spatial distributions of hydraulic variables (depth, velocity, and stream power) and morphologic variables (total concentration, total sediment yield, and elevation changes) for $RI_1 = 50$ mm/h of Case 5 are presented in Figure 6. Figures 6a–6c correspond to the time at flow steady state. In the spatial distribution of all of these flow variables, a similar pattern i.e., higher magnitudes in the channel network and lower values in the headwater areas, is observed from the time of concentration until the rainfall cessation. More specifically, in most regions of the domain, except for the flow convergence trough, the stream power barely exceeds a predefined threshold value needed to trigger overland flow-induced erosion. Thus, the

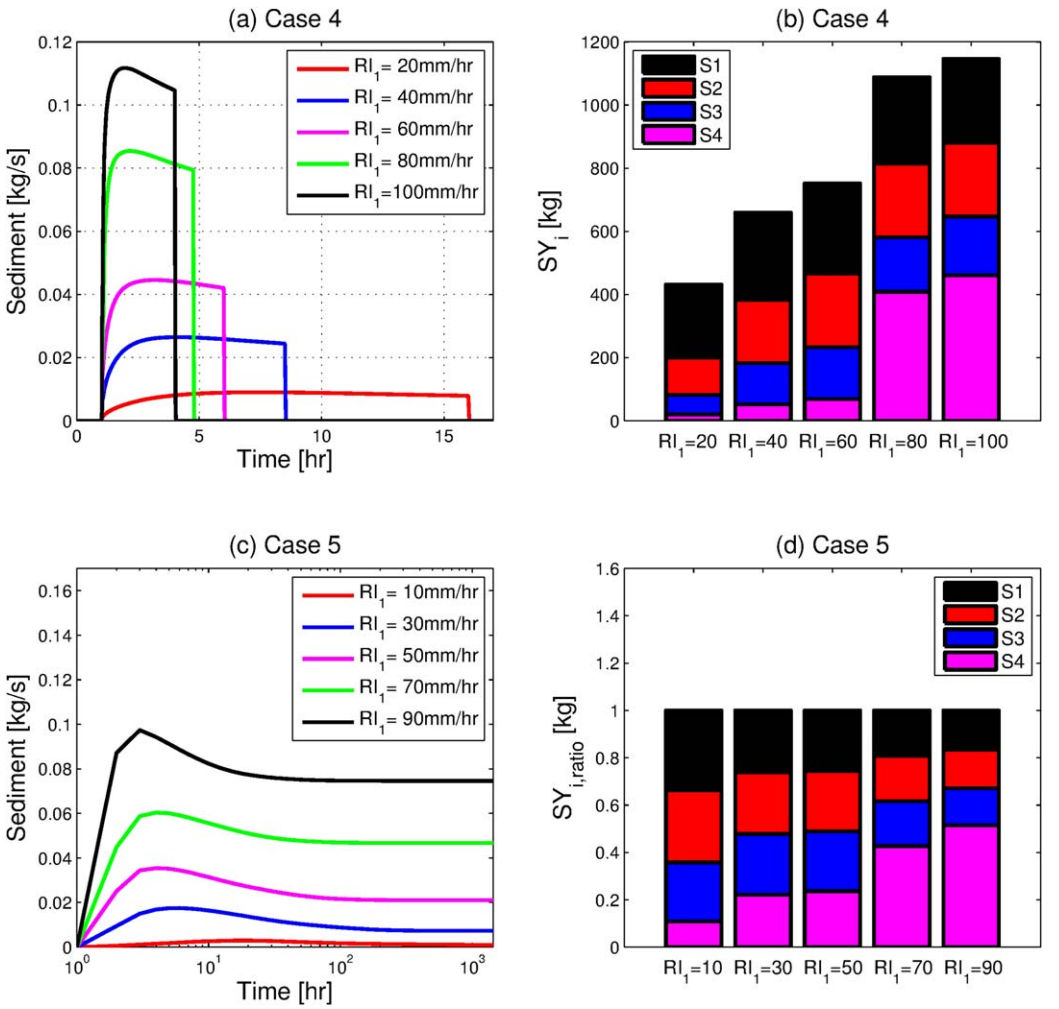

Figure 5. The simulated sedigraphs for (a) Case 4 and (c) Case 5. (b) The partition of sediment yield into absolute fractions corresponding to the four particle sizes (S1–S4) for Case 4. (d) The ratio of sediment yields corresponding to the four particle sizes (S1–S4) for the total sediment yield for Case 5.

predominant controller in such upland areas is raindrop impact and this phenomenon becomes more significant for cases with the smaller rainfall magnitudes.

Conversely to the temporal invariance of the flow state, the spatial patterns of morphologic variables continuously change until the steady state is reached. Initially, the rainfall-induced (re)detachment rates are spatially uniform but as flow depth becomes spatially variable, relatively higher detachment rates occur in the upland areas (not shown). The deposited mass increases with time and plays a role of shield in these upland areas, resulting in less erosion. To demonstrate the temporal transitions of morphologic variables, the simulated values are compared for two time instants: Figures 6d–6f correspond to the peak of sediment yield and Figures 6g–6i correspond to its steady state (these two critical times will be further compared in section 3.5). As seen from these two sets of subplots, sediment concentrations decrease from the peak yield time to the steady state, and they are particularly high in the area of flow convergence. In contrast, the deposited mass temporally increases and is higher in the headwater areas and hillslope midline regions due to their low stream power. Sediment shield in the channel areas, where flow driven entrainment dominates among sediment source procesess, is not as protective as in upland areas where raindrop-induced detachment dominates. Last, the elevation changes are computed to investigate regions where the domain eroded (negative magnitudes) or sediment deposition took place (positive magnitudes). Overall, large areas have eroded in the domain, with particularly high erosion rates in steeper regions. The amount of erosion has consistently increased with the rainfall duration (Figure 6f versus Figure 6i). The relative contribution of

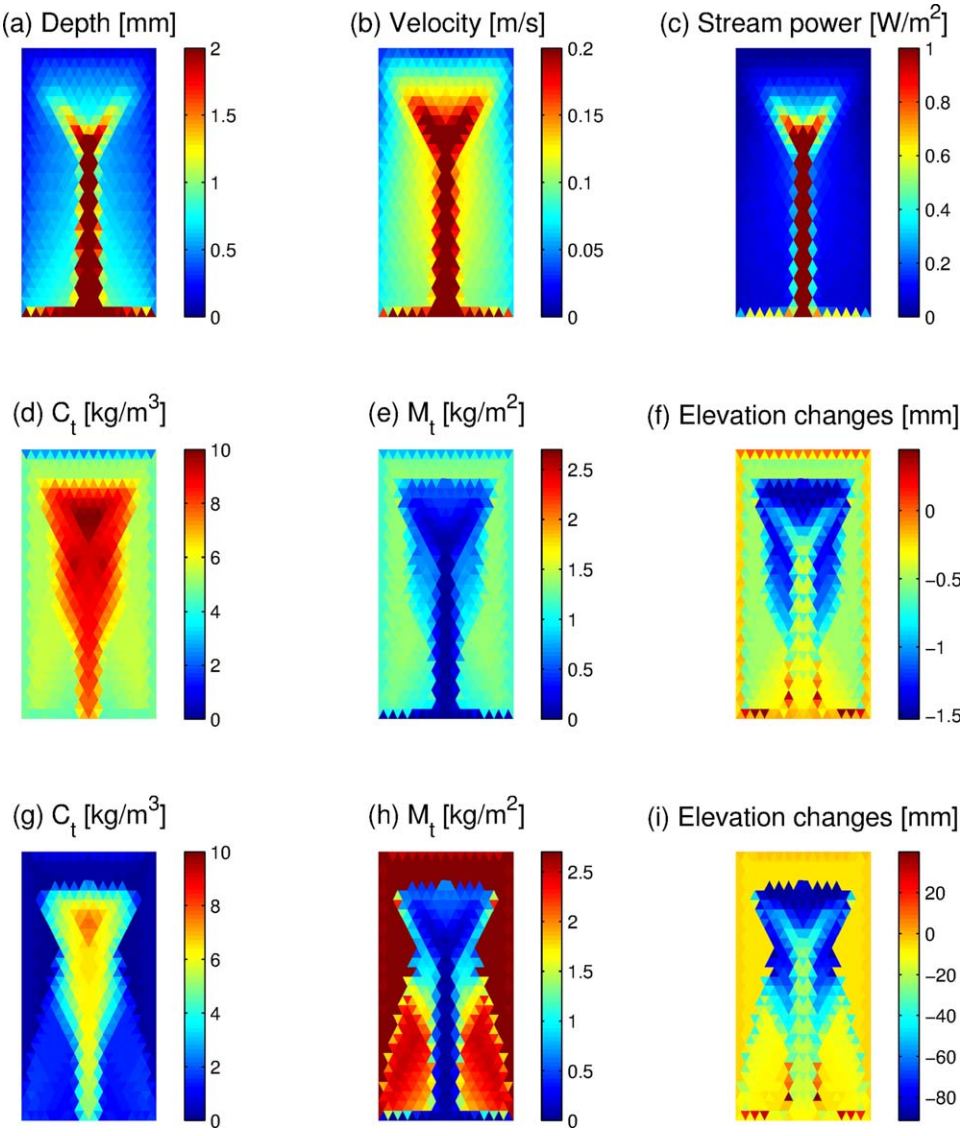

Figure 6. Spatial distributions of depth, velocity, stream power, total concentration, total sediment yield, and elevation changes for $RI_1 = 50$ mm/h of Case 5. (a–c) Correspond to the time at flow steady state; (d–f) correspond to the time at sediment yield peak (hour 4); and (g–i) correspond to time at sediment yield steady state (hour 163). In Figure 6i, positive values denote deposition and negative values imply erosion. C_t is the total sediment concentration and M_t is the total deposited mass.

the both types of erosion processes to total soil erosion is further shown in Figure S1 of the supporting information.

3.3. Variations of Sediment Yield for the Same Flow Volume

Several of the presented simulation results vividly demonstrate that there can be a considerable variation in sediment yield despite the same rainfall/runoff volume. One example of the variation is illustrated in Figures 5b and 5d with the partition of sediment yield into absolute (Figure 5b) or relative (Figure 5d) fractions corresponding to the four particle sizes (S1 through S4). An important feature of Case 4 is that despite the same runoff volume, the total sediment yield for $RI_1 = 100$ mm/h is almost three times higher than that for $RI_1 = 20$ mm/h (specifically, 431.7 versus 1146.2 kg). Such a large difference is mainly attributable to the high erosion loss of large-sized particles, which can be flushed from the deposited area when flow energy increases and thus transport mode changes from raindrop-induced saltation to flow driven saltation [*Kinnell*, 2009]. Similarly, the results in Figure 5d show that higher rainfall intensities result in progressively larger

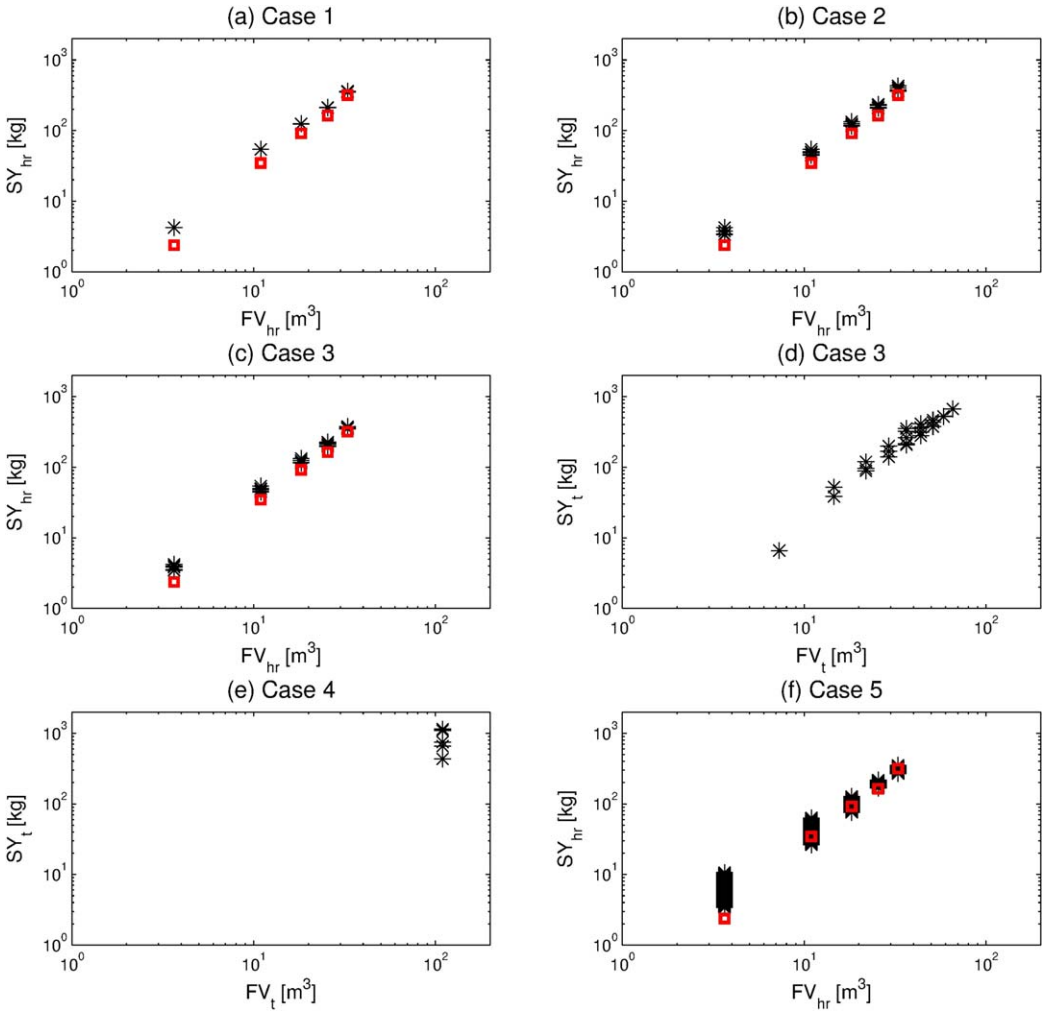

Figure 7. Flow volume (*FV*) plotted against sediment yield (*SY*) for all simulation cases. *FV* and *SY* are computed by integrating the flow and sediment rates of the corresponding hydrographs and sedigraphs. The red squares correspond to the first rainfall event (1 h duration, Cases 1, 2, and 3) or the first simulation hour (Case 5), for which the initial condition of soil bed was not "disturbed" (i.e., intact soil bed condition). Black stars correspond to either the second event ((a–c) Cases 1, 2, and 3), the entire single event ((d and e) Cases 3 and 4), or hourly volumes ((f) Case 5). Specifically, Figures 7d and 7e illustrate FV_t and SY_t that were computed for the entire simulation period of Cases 3 and 4 to ensure the same runoff volume. Figure 7f illustrates a regression between hourly sediment yield (SY_{hr}) and flow (FV_{hr}) of Case 5.

flow rates sufficient to entrain and move larger particles, giving rise to high nonlinearities of the total (and relative, partitioned) sediment yields.

While the dependence on rainfall rate has been long discussed in literature [*Edwards and Owens*, 1991; *Romkens et al*., 2001; *Abu Hammad et al*., 2006; *Ahmadi et al*., 2010; *Svoray and Ben-Said*, 2010], the results of this study address the importance of additional mechanisms that can cause similar conditions of non-uniqueness. Figure 7 summarizes the addressed variability by displaying event runoff volume versus the corresponding sediment yield for all of the considered simulation Cases. The initial condition of soil bed at the simulation start is "intact," i.e., soil that has not yet been disturbed. This corresponds to fairly low erodibility of the soil bed, leading to relatively low erosion. This is opposite to the effect of a "loose" soil condition that had been perturbed by a preceding rainfall event prior to the onset of a subsequent event (Cases 1–3, 5). Thus, the sediment yields for two events can be different, while corresponding to the same flow volume (e.g., Figures 7a–7c).

As a follow up conclusion based on the above inference, the eroded material generated during the first hour should be progressively smaller than sediment flux leaving the basin during later hours. Consistently with the logic, this is shown in Figures 7a–7c. However, an additional notable result in Figure 7f is that *SY*

Table 3. Variations of Sediment Yield V_{SY} (%) for All Cases Shown in Figure 7 With Respect to the Same Volume of Rainfall Corresponding to Either the Second Event (Cases 1, 2, and 3 in Figures 7a–7c), the Entire Single Event (Cases 3 and 4 in Figures 7d and 7e), or Hourly Volumes (Case 5 in Figure 7f)[a]

Rain Volume (mm)	Case 1	Case 2	Case 3	Case 4	Case 5	Rain Volume (mm)	Case 3
10	0.36	26.64	21.20	–	214.23	40	35.97
30	0.15	21.59	21.41	–	140.88	60	34.32
50	0.44	15.50	15.24	–	68.74	80	42.62
70	1.15	13.79	14.52	–	29.34	100	69.21
90	3.05	18.98	7.88		30.55	120	47.79
300	–	–	–	165.53	–	140	24.02
						160	0.97

[a]The last two columns represent variations illustrated in Figure 7d.

corresponding to later hours can be smaller than that for the first simulation hour. This result is of interest because in conditions of a relatively loose, deposited soil bed material, the erosion loss becomes smaller than that for soil in intact condition that exhibits low detachability. Such an outcome indicates that there exists a mechanism that hampers progressively higher erosion after soil particles have been moved from their original locations and some of the sediment mass has been deposited at downstream locations. This study argues that the mechanism is mainly attributed to the development of a surface shielding layer that protects underlying soil, thereby counteracting the effect of an increasing amount of loose material.

For all of the simulated Cases, a statistical metric is introduced to illustrate how a given precipitation scenario affects the variation of eroded sediment mass. Given the same rainfall volume, the variation of sediment yield mass V_{SY} (in percent) is defined as

$$V_{SY} = \frac{SY_{\max} - SY_{\min}}{SY_{\min}} \times 100 \ , \tag{1}$$

where the subscripts "max" and "min" refer to maximum and minimum values, respectively, among sediment yields (depicted as black stars in Figure 7, i.e., excluding the red squares) for the same flow volume. Table 3 shows the computed values of V_{SY} for all Cases shown in Figure 7. According to these estimates, the range of nonuniqueness caused by the effects of the time lag between two successive events of the same magnitude is extremely small (less than 3%, Case 1). Conversely, preevent sediment dynamics, as affected by magnitude of a previous rainfall event, can result in *SY* variations ranging from 7.9 to 26.6 % (Cases 2 and 3). Even larger variations in the total or hourly *SY* can occur in Cases 4 and 5, implying that longer intervals of coupled flow-sediment dynamics are likely to exhibit a more pronounced nonunique behavior in response to the same input.

The last two columns of Table 3 illustrate the erosion response based on estimates in Figure 7d, which show the total sediment yields associated with 2 h rainfall periods; *SY* variations were subsequently computed for the same rainfall volume (Case 3). Additionally, if one separately examines sequences of either increasing or decreasing rainfall magnitude in Case 3, the total *SY* corresponding to the sequence with an increasing trend is always greater than that for a sequence of events with decreasing magnitude. The corresponding variability of the total yield for the same rainfall volume was computed by comparing 10 subcase sets with both increasing and decreasing trends (e.g., one of the sets consists of two subcases, i.e., $RI_1 = 10$, $RI_2 = 30$, and $RI_1 = 30$, $RI_2 = 10$ mm/h, etc.), which resulted in the range from 1.0 to 36% (not shown). This variability indicates that depending on whether a storm interval with a higher erosive power occurs at the beginning or the end and depending on how significantly soil bed is perturbed during or prior to that, the prediction of the total sediment loss is strongly affected. In the context of the considered scenario of a continuous 2 h storm (Case 3), a higher rainfall during the second hour (applied in conditions of soil that was perturbed by the rainfall of the first hour) implies a larger erosion capacity. A similar conclusion was obtained experimentally by *Romkens et al.* [2001] for the case of 2% slope. However, an opposite result was obtained for the other two slopes used by the same authors: a decreasing precipitation rate yielded a larger sediment loss. This was primarily attributed to surface rilling, which was more severe for a decreasing storm rate, and to surface sealing, which is unlikely to occur for an initial rainfall of a higher intensity. Although the numerical model used here does not consider the processes of sealing or rill formation, another

considerable issue associated with this disparity is in the fact that the study of *Romkens et al*. [2001] did not use particles of larger sizes, being only constrained to 98% of clay and silt. Due to the imposed short time scale of the experiment (~6 h) and the used particle sizes, the development of a shielding layer was unlikely to occur.

3.4. Initialization Effects on the Nonuniqueness of Sediment Yield

The presented results suggest that the initial states of the domain in terms of distributions of flow characteristics and deposited mass can contribute to explaining the processes of sediment dynamics and the inferred nonuniqueness of *SY*. Specifically, Cases 1, 2, and 3 were designed so that first rainfall event generates varying initializations of hydraulic and morphologic variables for the second event. For Case 1, these were flow depth, velocity, and stream power; for Case 2, different distributions of deposited mass were generated; and for Case 3, different flow characteristics as well as sediment concentration and deposited mass were targeted. Basin geomorphic response only to the second event will be emphasized in the analysis.

In Case 1, the total sediment yields generated by the second event ($SY_{t,2}$) for the same rainfall magnitude of the first event (i.e., individual values on the *x* axis in Figure 7a) are almost unique (less than 3% variations). The sediment partition into the fractions corresponding to the four particle sizes for the second event ($SY_{i,2}$) also does not vary significantly, despite the wide range of initial states of flow depth or velocity (not shown). Specifically, the initial flow depth averaged over the domain before the commencement of the second event ranges between 10^{-3} m, for smaller T_b magnitudes (less than 15 min), and 10^{-6} m, for larger T_b. The general agreement of rainfall or overland flow-driven erosion processes is that the flow depth plays two conflicting roles: it positively impacts fluvial erosion through enhanced stream power; however, by forming a water shield, deeper flow hampers erosion by rainfall detachment [*Laws and Parsons*, 1943; *Mutchler and McGregor*, 1983; *Proffitt et al*., 1991; *Gabet and Dunne*, 2003; *Gao et al*., 2003]. The obtained outcome of Case 1 is because the effects of water depth are very minor: the domain is of zero order and therefore there is no sufficient flow accumulation. While the domain conditions represent an idealized simulation case, the same phenomenon can be expected in headwater areas of complex topography exhibiting a small fraction of surface runoff detention.

In Cases 2 and 3, different spatial compositions of bed in terms of original, "intact" soil and nonlocal sediment material transported and deposited locally prior to the second event were obtained. In order to capture the differences between the corresponding composition states, particle-size distributions of the deposited mass prior to the second event ($M_{i,2}^{ini}$) are averaged spatially and presented in Figure 8 (for $RI_2 = 50$ mm/h only). Higher magnitudes of $M_{i,2}^{ini}$ represent a larger mass of deposited loose material. Depending on preceding rainfall (i.e., the magnitude of RI_1), the local surface condition of soil can be partially altered; 5 (smallest rainfall rate) to 20% (highest rainfall rate) of initially intact soil are changed to the deposited soil condition. The deposited sediment also exhibits spatially varying PSDs, which can be very different from the uniform distribution of sizes in the original, intact soil. As seen in Figures 8b and 8d, a smaller rainfall intensity of the first event leads to a PSD similar to that of the original soil. Conversely, larger magnitudes of the first event transform the composition of the surface soil dramatically, which can become composed of predominantly coarser particles (see Figures 8b and 8d). It can be also inferred that as $M_{i,2}^{ini}$ increases, sediment yield ($SY_{i,2}$) also grows initially because the deposited soil material has a higher erodibility, as compared to the original soil. However, $SY_{i,2}$ exhibits a maximum at lower magnitudes of the deposited soil material and shows a decay for larger $M_{i,2}^{ini}$ (for both Cases 2 and 3, Figures 8a and 8c). A similar pattern of dependence is obtained for other magnitudes of RI_2 (not shown). Such a peculiar behavior is explained by the growing fraction of coarser particles that have high settling velocities: through their deposition, a surface shield is created. Since large particles (which are otherwise "loose") cannot be easily entrained, the formation of such a shielding layer protects the underlying intact soil and impedes the process of erosion.

3.5. Patterns of Evolution of Sediment Yield and Critical Time Scales

Morphologic variables characterizing sediment content in a water column and deposited area are key indicators for inspecting the variation of sediment yield. The long-term simulation of Case 5 is used to detect phases of nonuniqueness of erosion and deposition processes, relate them to morphologic variables, and find the time scales describing characteristic transitions of sediment generation within a watershed.

The nonunique property of erosion and sediment transport of this particular simulation case has already been illustrated by the sedigraph in Figure 5c. During the continuous rainfall, water flow early achieves

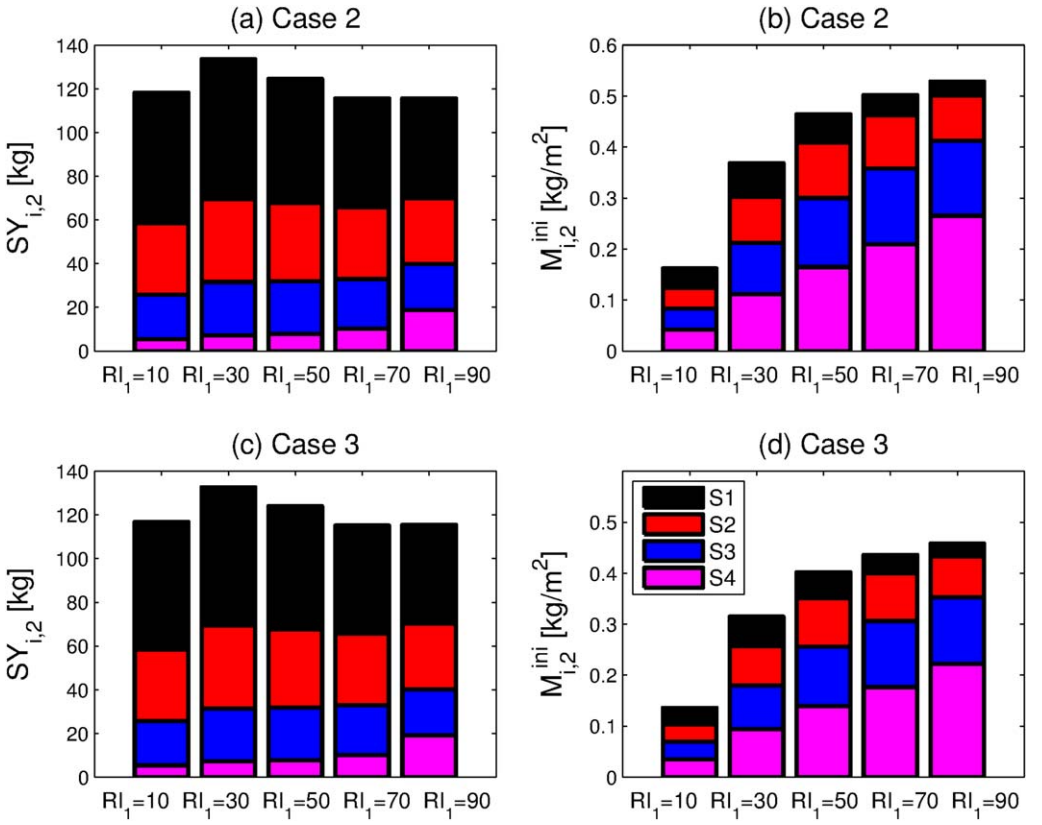

Figure 8. The partition of sediment yield ($SY_{i,2}$) generated by the second event into relative fractions corresponding to the four particle sizes (S1–S4) for (a) Case 2 and (c) Case 3; and the partition of spatially averaged deposited mass immediately prior to the second event ($M_{i,2}^{ini}$) for (b) Case 2 and (d) Case 3. All subplots correspond to the results of $RI_2 = 50$ mm/h.

steady state (∼4 to 7 min after the start) and maintains it over an entire simulation period, as seen in Figure 9a. Initially, the eroded materials yielded by the catchment are represented by smaller, silt-size sediments that lead to a peak in sediment yield rate at an early stage, which is however significantly delayed as compared to flow peak (∼ 4 h after the start). After the peak, the sediment rate decreases and asymptotically approaches the steady state. This dynamic, unsteady evolution is illustrated in Figure 9b for $RI_1 = 50$ mm/h. As seen, both $SY_{t,hr}$ and $C_{t,hr}^{ini}$ follow the described increasing-decreasing-steady state trend, while $M_{t,hr}^{ini}$ exhibits an increasing-steady state trend. The transitions to the steady state for these three metrics are in general accordance and the determination of the transient time scales thus should play a crucial role in understanding the nonunique property of the erosional response.

It has been practically infeasible for experimental studies to observe such a pattern of dynamics over the long term. However, previous research based on results of a mechanistic numerical model applied in a limited range of topographic and flow conditions (i.e., one-dimensional domains and fixed advection flow depths and velocities) also showed the existence of peak and steady state in the composition of sediment discharged by rain-impacted flow [*Kinnell*, 2006; *Sharmeen and Willgoose*, 2006; *Willgoose and Sharmeen*, 2006; *Kinnell*, 2009, 2012]. Similarly to the present study, the phenomenon was attributed to the development of an "impediment" effect to the sediment discharge, controlled by slowest moving particles. More specifically, the effect was achieved by considering the amount of coarser material mass lifted into flow and travel distance of the coarser particle by tracking its pathline, which thus excluded an explicit representation of interactions among particles of different sizes. Conversely, the H-R formulation dynamically computes the advection flow velocity and the magnitude of source terms for all particles at a given location in space and time, thereby relating the representation of local interactions to the integrated response. This offers a different physical interpretation of the peak and steady-state phenomenon, explicitly attributing it to the effect of shielding. The property of nonuniqueness is also shown to operate at the scales of a natural headwater catchment.

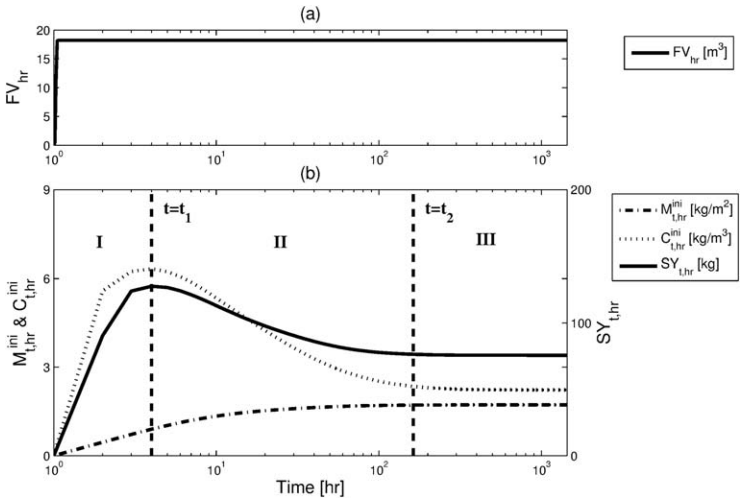

Figure 9. An illustration of the dynamic, unsteady evolution of erosion and sediment transport response to a continuous rainfall of $RI_1 = 50$ mm/h simulated in Case 5. The temporal evolution of (a) the hourly flow volume (FV_{hr}) and (b) the hourly instantaneous, the spatially averaged total concentrations ($C^{ini}_{t,hr}$) and the total deposited mass ($M^{ini}_{t,hr}$) as well as the total sediment yield ($SY_{t,hr}$). The left axis is used for $M^{ini}_{t,hr}$ and $C^{ini}_{t,hr}$, while the right axis is used for $SY_{t,hr}$. The two time scales, t_1 and t_2, are identified with the two vertical dashed lines; the three corresponding phases (I, II, and III) are also illustrated. The results obtained for the other rainfall intensities and also specific for each particle size are provided in the supporting information (section S.1).

Two critical characteristic periods, the time to peak (t_1) and the time to steady state (t_2) are defined here by using the simulated sediment yield series. The interval t_1 is defined as the period to a maximum value of SY_{hr} and t_2 is defined as the largest time that satisfies the following two criteria:

$$\frac{dSY_{hr}(t_2)}{dt} < \epsilon \quad \text{and} \quad SY_{hr}(t_2) > 1.01 SY_{hr}(t_{\text{end}}) \ , \tag{2}$$

where t is time; $SY_{hr}(t)$ is the hourly sediment yield at time t; t_{end} is the time at the end of simulation (60 d) at which steady state is achieved for most simulations (except for the case with $RI_1 = 10$ mm/h in which a much longer rainfall is needed); and ϵ is a tolerance value assumed to be 10^{-4} in this study. The above criteria are chosen so as to avoid numerically unrealistic large values in t_2 estimation.

Based on these criteria, both the time to peak (t_1) and the time to steady state (t_2) are computed and illustrated in Figure 9 as well as Figure S2 in the supporting information. The two time scale values are qualitatively related to a given precipitation input and sediment size: the smaller the rainfall rate and the heavier a given particle is, the longer it takes to reach t_1 and t_2. One of this findings, i.e., t_2 dependency on particle sizes, was also observed in a flume study [*Jomaa et al*., 2013]. This observation can be explained by introducing the dimensionless Shields parameter (τ_*). The Shields parameter, defined as the ratio of the drag force to the submerged weight of a particle, describes the extent of forcing to resistance for sediments:

$$\tau_* = \frac{\tau}{(\rho_s - \rho_w) g D} \ , \tag{3}$$

where τ is the shear stress; g is the acceleration constant due to gravity; and D is the diameter of a particle. The time t_1 and t_2 time scales are log linearly and negatively related to the spatially averaged Shields parameters for both S1–S4 (Figure 10). The obtained relationships confirm that a higher magnitude of rainfall forcing perturbs soil bed more rapidly, achieving earlier peak time and steady state. The supporting information provides further analysis of the two time scales with respect to the rainfall intensities and particle sizes (see section S2 of the supporting information).

A physical interpretation of the two time scales leads to identification of three characteristic regimes of geomorphic response: flow-limited, source-limited, and steady-state regimes.

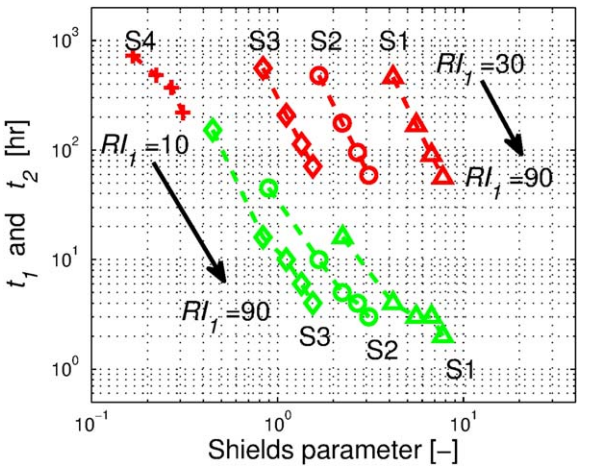

Figure 10. The Shields parameter related to the two time scales, the time to peak (t_1) and the time to steady state (t_2): the green dashed lines correspond to t_1, while the red dashed lines correspond to t_2. For S4 ("+" symbol), t_1 and t_2 are overlapped and for RI_1 = 10 mm/h, the steady state is not reached.

1. The flow-limited regime, time-$\leq t_1$. During an early stage of rainfall, there is an increase of loose sediments that are likely to be eroded and transported by the flow. If it rains continuously, the sediment contained in the deposited layer and water column also grows, resulting in larger local erosion and yield at the basin outlet. In this regime, the sediment source is always sufficient and does not limit entrainment into the water column. Larger runoff or flow would cause higher erosion and the basin yield.

2. The source-limited regime, $t_1 <$ time $\leq t_2$. Continuing rain keeps driving the processes of detachment, entrainment, and deposition, but the geomorphic response changes. Even though the total deposited mass is continuously increasing, the basin sediment yield no longer grows after t_1. This is because of the dynamic evolution of a shielding layer formed by larger, heavier particles. The yield of smaller-sized particles that can be easily eroded and transported is becoming constrained by their availability across the domain, as these particles had been mostly flushed out of the basin prior to the occurrence of t_1. The yield therefore would not respond positively to an increase in runoff/flow depth.

3. The steady-state regime, time $> t_2$. The ratio between sediment originating from the initially "intact" soil and deposited mass as well as the partition of each particle size within the deposited soil become time invariant, reflecting "stabilization" of the soil bed. For any subsequent hours of the same rainfall forcing, the unit response will be identical. An increase in the rainfall forcing will however drive an unsteady regime that will cause the occurrence of all three regimes of sediment dynamics, albeit with different characteristic time scales.

3.6. Patterns of Temporal Evolution Specific to Particle Sizes

Figure 11 is intended to facilitate the understanding of temporal evolution of the spatially averaged concentration of individual particle size $C^{ini}_{i,hr}$ and deposited mass $M^{ini}_{i,hr}$ (the subscript "i" denoting the four particle sizes, S1–S4). The occurrence of the three characteristic regimes for these variables is also illustrated. The cumulative SY_{hr} are shown with respect to $C^{ini}_{i,hr}$ and deposited mass $M^{ini}_{i,hr}$. Overall, the evolution patterns of $C^{ini}_{i,hr}$ and $M^{ini}_{i,hr}$ are contrasting: as the particle size increases, smaller concentrations and higher deposited masses are simulated; a wide range of concentrations occurs during an early simulation period and a nearly uniform magnitude is reached at steady state. An opposite evolution pattern takes place for the deposited mass. The particle-size specific characteristics of the three regimes can be described as follows. (1) Over the period near the simulation start, $M^{ini}_{i,hr}$ corresponds to the particle-size distribution of the original soil. Such a period is longer for smaller RI (see Figure S3 in the supporting information) because the limited erosion capacities resulting from smaller rainfall/runoff rates lead to a delayed initiation of selective erosion processes. Over the same period, a similar mass of each particle size on the bed becomes entrained but heavier materials are deposited at a larger rate, resulting in higher concentrations of smaller particles. In contrast, the sediment sources for all particle types in the bottom and the water column are increasing until the timing of sediment yield peak. (2) After the peak time, lighter particles are still preferably eroded and transported within the domain without a significant deposition. Heavier particles start covering the underlying original ("intact") soil and thus, the availability of lighter sediment becomes restricted by the deposition of heavier sediment material. This phenomenon is graphically represented as the abrupt decrease of availability of lightest particles ($C^{ini}_{i,hr}$ and $M^{ini}_{i,hr}$), while a gradual increase of the heaviest type (Figure 11). At this period, most of particles that are available for erosion are the largest particle type, which results in the

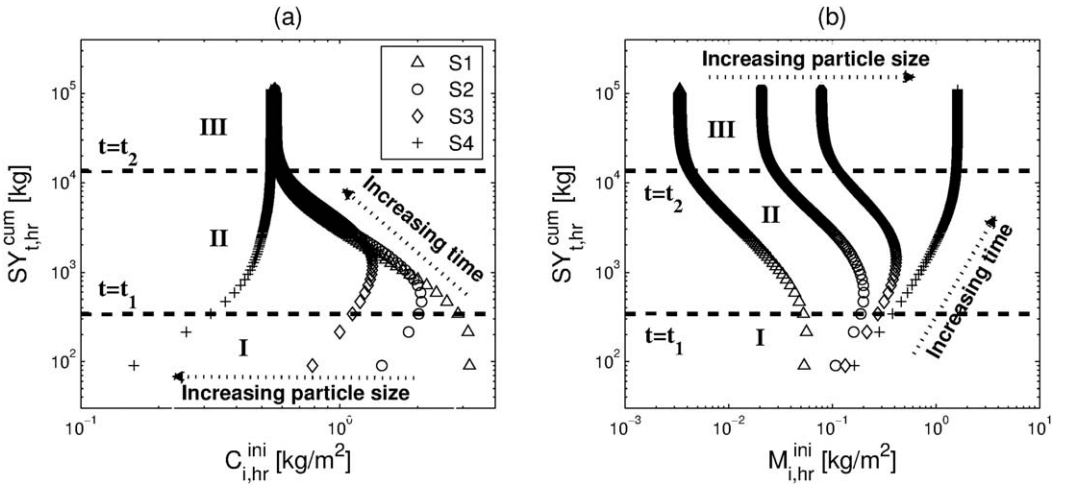

Figure 11. An illustration of dynamic, unsteady evolution of erosion and sediment transport response to a continuous rainfall of $RI_1 = 50$ mm/h simulated in Case 5. The cumulative total sediment yield resolved at the hourly scale $SY^{cum}_{t,hr}$ plotted against the spatially averaged, type-specific (for the four particle sizes, S1–S4) (c) concentration $C^{ini}_{i,hr}$ and (d) deposited mass $M^{ini}_{i,hr}$. The two time scales, t_1 and t_2, are identified with the two horizontal dashed lines; the three corresponding phases (I, II, and III) are also illustrated. The results obtained for the other rainfall intensities and also specific for each particle size are provided in the supporting information (section S.2).

retardation of all relevant erosion processes. The temporal variation of $C^{ini}_{i,hr}$ and $M^{ini}_{i,hr}$ is more significant for smaller *RI* (Figure S3 in the supporting information). (3) During the steady-state regime, the variations of morphologic variables stabilize: a nearly uniform concentration for all particle sizes in the flow water column is attained; the fractions in the deposited mass however vary by several orders of magnitude (Figure 11). These stable morphologic conditions define the continuing steady-state response of the basin. The supporting information provides an additional analysis of the effects of rainfall intensity on the particle-size specific dynamics (section S3 of the supporting information).

4. Summary and Conclusions

Nonuniqueness of sediment yield for a given runoff volume has been empirically observed and obtained in numerical modeling studies, being generally attributed to nonlinearities of watershed process interactions. The objective of this study is to offer a mechanistic explanation of the nonuniqueness occurring for a particular set of conditions related to size-selective erosion processes. In order to facilitate the analysis and explore internal dynamics, a series of modeling scenarios for a zero-order watershed is developed to generate an ensemble of runoff and sediment responses simulated in a controlled fashion, i.e., without explicit representation of the processes of infiltration and subsurface moisture dynamics. The series of simulation cases are designed so that rainfall intensity, duration, and lag time between successive events are varied. The anticipated outcome of such a design is that a preceding rainfall event creates a "perturbation" of soil substrate and flow regime prior to the onset of a subsequent rainfall event. Specifically, the first rainfall event generates varying initializations of hydraulic and morphologic variables (Cases 1, 2, and 3). These are flow depth, velocity, and stream power (Case 1); different distributions of deposited mass are generated (Case 2); and different flow characteristics as well as sediment concentration and deposited mass are produced (Case 3). Simulations of response to long-term precipitation are represented to resolve continuously varying morphologic bed conditions for a steady-state hydraulic flow regime (Cases 4 and 5).

The generated different initial conditions change the particle-size distribution of the soil substrate, which may form a shielding layer composed of larger particles. One of the outcomes is that unless the initial conditions of flow and sediment are identical, the same volume of runoff (produced at the same rate) can generate different total sediment yields. For example, the variation of sediment yield for the case where time lag between two events was varied (Case 1) is nearly zero (less than 3%), because of the limited change in the initial condition. However, variations exhibited by the remaining simulation cases reach up to ~200%. In the case when two rainfall pulses with different rainfall intensities are used (Case 3), the sediment yield is

greater for a sequence of rainfall events with increasing magnitudes, as compared to decreasing magnitudes.

The shield formation by relatively larger particles can be one of the significant controllers of erosion and net sediment transport at the event scale; the cycle of shield formation and destruction is likely to be a strong contributor to the nonuniqueness of erosion dependence on runoff. The temporal development of the shielding layer determines the amount of sediments in the flow water column and areas of deposition, resulting in the dynamic, unsteady variation of sediment yield. For a long-term simulation with continuous rainfall, the peculiar feature of sediment yield is the existence of maximum, before a steady state is reached. The two identified time scales, i.e., the time to peak (t_1) and the time to steady state (t_2) distinguish the corresponding transitions that help addressing the nonuniqueness property of sediment yield from a physical standpoint. Specifically, the time scales imply the existence of three characteristic periods that correspond to the flow-limited, source-limited, and steady-state regimes. The flow-limited regime occurs during early stages of rainfall. Continuous forcing leads to an increase of watershed areas where sediment is detached from the soil surface by rainfall or entrained by the flow, resulting in a net increase of erosion. In this regime, the sediment source is sufficient and thus a larger forcing would lead to higher erosion. The source-limited regime corresponds to the time period between t_1 and t_2. During this time, the total deposited mass that has higher erodibility than the original "intact" soil is continuously increasing but the domain sediment yield diminishes after t_1. This occurs because of the dynamic evolution of a shielding layer formed by larger particles—they cover the underlying intact soil thereby causing a concurrent reduction of availability of lighter sediment. During the steady state after t_2, the soil bed condition, i.e., the ratio of the amount of intact and loose materials, and the component substrates inside the deposited area become stabilized and time invariant. The stabilized soil condition always provides an identical response to the same forcing. Therefore, a unique relationship between rainfall forcing and generated sediment yield is attained at this phase.

Soil erosion and sediment transport are complex phenomena and it has been practically impossible to fully incorporate all relevant details in numerical models. This study addressed only those erosion processes that are perceived to be essential in a zero-order catchment: rainfall-induced detachment and overland flow-induced entrainment of soil particles, their deposition due to gravity, and shield effects by both larger particles and flow depth. These processes are simultaneously computed responding to a detailed representation of flow motion. Other related processes depending on a degree of soil saturation, slaking, dispersion, crusting, and rill formation are not taken into account because of the intricacies of relevant theories and existing parameterizations. Despite the simplified nature of the erosion processes and the implications of underlying assumptions, the obtained results simulated for a zero-order catchment that represent headwater areas of natural watersheds are considered to be physically sound. Two major conflicting effects of the shielding layer impacting nonuniqueness of sediment yield have been captured: a positive contribution to erosion, because of supply of highly erodible sediment, and erosion impediment, because of constrain on availability of lighter particles. One of the practical implications of this study is that except for cases when original soil layer is entirely covered by loose materials (e.g., headwater alluvial gullies), accurate, deterministic short-term predictions of geomorphic events from headwater areas may never become a tractable problem. The latter would require an unrealistically detailed spatial characterization of particle-size distribution prior to precipitation events.

Acknowledgments
This study was supported by the NSF grant EAR 1151443. The authors thank Calvin W. Rose, Seifeddine Jomaa, and an anonymous reviewer for a constructive criticism of the paper during the review process.

References

Abbott, M. B. (1974), Continuous flows, discontinuous flows and numerical analysis, *J. Hydraul. Res.*, *12*(4), 417–467.
Abu Hammad, A. H., T. Børresen, and L. E. Haugen (2006), Effects of rain characteristics and terracing on runoff and erosion under the Mediterranean, *Soil Tillage Res.*, *87*(1), 39–47.
Ahmadi, A., M. R. Neyshabouri, H. Rouhipour, H. Asadi, and M. Irannajad (2010), Factors and mechanisms influencing interrill erodibility at different rainfall intensities, *J. Food Agric. Environ.*, *8*(2), 996–999.
Armstrong, A., J. N. Quinton, B. C. P. Heng, and J. H. Chandler (2011), Variability of interrill erosion at low slopes, *Earth Surf. Processes Landforms*, *36*(1), 97–106.
Armstrong, A., J. N. Quinton, B. C. P. Heng, and G. C. Sander (2012), Processes controlling the development of a shielding layer on natural soil, *Eur. J. Soil Sci.*, *63*(1), 54–64.
Cheng, N. (1997), Simplified settling velocity formula for sediment particle, *J. Hydraul. Eng.*, *123*(2), 149–152.
Cohen, S., G. Willgoose, and G. Hancock (2009), The mARM spatially distributed soil evolution model: A computationally efficient modeling framework and analysis of hillslope soil surface organization, *J. Geophys. Res.*, *114*, F03001, doi:10.1029/2008JF001214.
Cohen, S., G. Willgoose, and G. Hancock (2010), The mARM3D spatially distributed soil evolution model: Three-dimensional model framework and analysis of hillslope and landform responses, *J. Geophys. Res.*, *115*, F04013, doi:10.1029/2009JF001536.

Cohen, S., G. Willgoose, and G. Hancock (2013), Soil-landscape response to mid and late Quaternary climate fluctuations based on numerical simulations, *Quat. Res.*, *79*(3), 452–457.
Defersha, M. B., and A. M. Melesse (2012), Field-scale investigation of the effect of land use on sediment yield and runoff using runoff plot data and models in the Mara River basin, Kenya, *Catena*, *89*, 54–64.
Defersha, M. B., S. Quraishi, and A. Melesse (2011), The effect of slope steepness and antecedent moisture content on interrill erosion, runoff and sediment size distribution in the highlands of Ethiopia, *Hydrol. Earth Syst. Sci.*, *15*, 2367–2375.
Edwards, W. M., and L. B. Owens (1991), Large storm effects on total soil erosion, *J. Soil Water Conserv.*, *46*(1), 75–78.
Fatichi, S., V. Y. Ivanov, and E. Caporali (2012), A mechanistic ecohydrological model to investigate complex interactions in cold and warm water-controlled environments: 1. Theoretical framework and plot-scale analysis, *J. Adv. Model. Earth Syst.*, *4*, M05002, doi:10.1029/02011MS000086.
Francipane, A., V. Y. Ivanov, L. V. Noto, E. Istanbulluoglu, E. Arnone, and R. L. Bras (2012), tRIBS-Erosion: A parsimonious physically-based model for studying catchment hydro-geomorphic response, *Catena*, *92*, 216–231.
Gabet, E. J., and T. Dunne (2003), Sediment detachment by rain power, *Water Resour. Res.*, *39*(1), 1002, doi:10.1029/2001WR000656.
Gao, B., M. T. Walter, T. S. Steenhuis, J. Y. Parlange, K. Nakano, C. W. Rose, and W. L. Hogarth (2003), Investigating ponding depth and soil detachability for a mechanistic erosion model using a simple, *J. Hydrol.*, *277*(1–2), 116–124.
Hairsine, P. B., and C. W. Rose (1991), Rainfall detachment and deposition: Sediment transport in the absence of flow-driven processes, *Soil Sci. Soc. Am. J.*, *55*(2), 320–324.
Hairsine, P. B., and C. W. Rose (1992), Modeling water erosion due to overland flow using physical principles: 1. Sheet flow, *Water Resour. Res.*, *28*(1), 237–243.
Hairsine, P. B., G. C. Sander, C. W. Rose, J. Y. Parlange, W. L. Hogarth, I. Lisle, and H. Rouhipour (1999), Unsteady soil erosion due to rainfall impact: A model of sediment sorting on the hillslope, *J. Hydrol.*, *220*(3–4), 115–128.
Hairsine, P. B., L. Beuselinck, and G. C. Sander (2002), Sediment transport through an area of net deposition, *Water Resour. Res.*, *38*(6), 22-1–22-7, doi:10.1029/2001WR000265.
Harmel, R. D., C. W. Richardson, K. W. King, and P. M. Allen (2006), Runoff and soil loss relationships for the Texas Blackland Prairies ecoregion, *J. Hydrol.*, *331*, 471–483.
Harmel, R. D., J. V. Bonta, and C. W. Richardson (2007), The original USDA-ARS experimental watersheds in Texas and Ohio: Contributions from the past and visions for the future, *Trans. ASABE*, *50*(5), 1669–1675.
Hayhoe, K., J. VanDorn, T. Croley Ii, N. Schlegal, and D. Wuebbles (2010), Regional climate change projections for Chicago and the US Great Lakes, *J. Great Lakes Res.*, *36*, 7–21.
Heilig, A., et al. (2001), Testing a mechanistic soil erosion model with a simple experiment, *J. Hydrol.*, *244*(1–2), 9–16.
Heng, B. C. P., G. C. Sander, and C. F. Scott (2009), Modeling overland flow and soil erosion on nonuniform hillslopes: A finite volume scheme, *Water Resour. Res.*, *45*, W05423, doi:10.1029/2008WR007502.
Heng, B. C. P., G. C. Sander, A. Armstrong, J. N. Quinton, J. H. Chandler, and C. F. Scott (2011), Modeling the dynamics of soil erosion and size-selective sediment transport over nonuniform topography in flume-scale experiments, *Water Resour. Res.*, *47*, W02513, doi:10.1029/2010WR009375.
Hogarth, W. L., C. W. Rose, J. Y. Parlange, G. C. Sander, and G. Carey (2004a), Soil erosion due to rainfall impact with no inflow: A numerical solution with spatial and temporal effects of sediment settling velocity characteristics, *J. Hydrol.*, *294*(4), 229–240.
Hogarth, W. L., J. Y. Parlange, C. W. Rose, G. C. Sander, T. S. Steenhuis, and A. Barry (2004b), Soil erosion due to rainfall impact with inflow: An analytical solution with spatial and temporal effects, *J. Hydrol.*, *295*(1–4), 140–148.
Ivanov, V. Y., E. R. Vivoni, R. L. Bras, and D. Entekhabi (2004), Catchment hydrologic response with a fully distributed triangulated irregular network model, *Water Resour. Res.*, *40*, W11102, doi:10.1029/2004WR003218.
Ivanov, V. Y., S. Fatichi, G. D. Jenerette, J. F. Espeleta, P. A. Troch, and T. E. Huxman (2010), Hysteresis of soil moisture spatial heterogeneity and the ''homogenizing'' effect of vegetation, *Water Resour. Res.*, *46*, W09521, doi:10.1029/02009WR008611.
Jomaa, S., D. A. Barry, A. Brovelli, G. C. Sander, J. Y. Parlange, B. C. P. Heng, and H. J. Tromp-van Meerveld (2010), Effect of raindrop splash and transversal width on soil erosion: Laboratory flume experiments and analysis with the Hairsine-Rose model, *J. Hydrol.*, *395*(1–2), 117–132.
Jomaa, S., D. A. Barry, B. C. P. Heng, A. Brovelli, G. C. Sander, and J. Y. Parlange (2012), Influence of rock fragment coverage on soil erosion and hydrological response: Laboratory flume experiments and modeling, *Water Resour. Res.*, *48*, W05535, doi:10.1029/2011WR011255.
Jomaa, S., D. A. Barry, B. C. P. Heng, A. Brovelli, G. C. Sander, and J. Y. Parlange (2013), Effect of antecedent conditions and fixed rock fragment coverage on soil erosion dynamics through multiple rainfall events, *J. Hydrol.*, *484*, 115–127.
Kim, J., V. Y. Ivanov, and N. D. Katopodes (2012a), Hydraulic resistance to overland flow on surfaces with partially submerged vegetation, *Water Resour. Res.*, *48*, W10540, doi:10.1029/12012WR012047.
Kim, J., A. Warnock, V. Y. Ivanov, and N. D. Katopodes (2012b), Coupled modeling of hydrologic and hydrodynamic processes including overland and channel flow, *Adv. Water Resour.*, *37*, 104–126.
Kim, J., V. Y. Ivanov, and N. D. Katopodes (2013), Modeling erosion and sedimentation coupled with hydrological and overland flow processes at the watershed scale, *Water Resour. Res.*, *49*, 5134–5154, doi:10.1002/wrcr.20373.
Kinnell, P. I. A. (1993), Interrill erodibilities based on the rainfall intensity flow discharge erosivity factor, *Aust. J. Soil Res.*, *31*(3), 319–332.
Kinnell, P. I. A. (2005), Raindrop-impact-induced erosion processes and prediction: A review, *Hydrol. Processes*, *19*(14), 2815–2844.
Kinnell, P. I. A. (2006), Simulations demonstrating interaction between coarse and fine sediment loads in rain-impacted flow, *Earth Surf. Processes Landforms*, *31*, 355–367.
Kinnell, P. I. A. (2009), The influence of raindrop induced saltation on particle size distributions in sediment discharged by rain-impacted flow on planar surfaces, *Catena*, *78*(1), 2–11.
Kinnell, P. I. A. (2012), Raindrop-induced saltation and the enrichment of sediment discharged from sheet and interrill erosion areas, *Hydrol. Processes*, *26*(10), 1449–1456.
Lane, L. J., M. Hernandez, and M. Nichols (1997), Processes controlling sediment yield from watersheds as functions of spatial scale, *Environ. Modell. Software*, *12*(4), 355–369.
Laws, J. O., and D. A. Parsons (1943), The relation of raindrop size to intensity, *Eos Trans. AGU*, *24*, 452–460.
Le Bissonnais, Y., A. Bruand, and M. Jamagne (1989), Laboratory experimental study of soil crusting: Relation between aggregate breakdown mechanisms and crust stucture, *Catena*, *16*(4–5), 377–392.
Le Bissonnais, Y., B. Renaux, and H. Delouche (1995), Interactions between soil properties and moisture content in crust formation, runoff and interrill erosion from tilled loess soils, *Catena*, *25*(1–4), 33–46.
Leendertse, J. J. (1967), Aspects of a computational model for long-period water wave propagation, *Memo. RM-5294-PR*, Rand Corp., Santa Monica, Calif.

Liggett, J. A. (1968), Mathematical flow determination in open channels, *J. Eng. Mech. Div. Am. Soc. Civ. Eng.*, *94*(EM4), 947–963.
Mamedov, A. I., C. Huangb, and G. J. Levy (2006), Antecedent moisture content and aging duration effects on seal formation and erosion in smectitic soils, *Soil Sci. Soc. Am. J.*, *70*, 832–843.
Misra, R. K., and C. W. Rose (1995), An examination of the relationship between erodibility parameters and soil strength, *Aust. J. Soil Res.*, *33*(4), 715–732.
Mutchler, C. K., and K. C. McGregor (1983), Erosion from low slopes, *Water Resour. Res.*, *19*(5), 1323–1326.
Nearing, M. A., G. R. Foster, L. J. Lane, and S. C. Finkner (1989), A process-based soil erosion model for USDA-water erosion prediction project technology, *Trans. ASAE*, *32*(5), 1587–1593.
Nearing, M. A., A. Kimoto, M. H. Nichols, and J. C. Ritchie (2005), Spatial patterns of soil erosion and deposition in two small, semiarid watersheds, *J. Geophys. Res.*, *110*, F04020, doi:10.1029/2005JF000290.
Nearing, M. A., M. H. Nichols, J. J. Stone, K. G. Renard, and J. R. Simanton (2007), Sediment yields from unit-source semiarid watersheds at Walnut Gulch, *Water Resour. Res.*, *43*, W06426, doi:10.1029/2006WR005692.
Notebaerta, B., G. Verstraetena, P. Wardb, H. Renssenb, and A. V. Rompaey (2011), Modeling the sensitivity of sediment and water runoff dynamics to Holocene climate and land use changes at the catchment scale, *Geomorphology*, *126*(1–2), 18–31.
Papanicolaou, A. N., J. T. Sanford, D. C. Dermisis, and G. A. Mancilla (2010), A 1-D morphodynamic model for rill erosion, *Water Resour. Res.*, *46*, W09541, doi:10.1029/2009WR008486.
Phillips, J. (2003), Alluvial storage and the long-term stability of sediment yields, *Basin Res.*, *15*, 153–163.
Pierson, F. B., C. W. Slaughter, and Z. K. Cram (2001), Long-term stream discharge and suspended-sediment database, Reynolds Creek Experimental Watershed, Idaho, United States, *Water Resour. Res.*, *37*(11), 2857–2861.
Polyakov, V. O., and M. A. Nearing (2003), Sediment transport in rill flow under deposition and detachment conditions, *Catena*, *51*, 33–43.
Proffitt, A. P. B., C. W. Rose, and P. B. Hairsine (1991), Rainfall detachment and deposition: Experiments with low slopes and significant water depths, *Soil Sci. Soc. Am. J.*, *55*(2), 325–332.
Proffitt, A. P. B., P. B. Hairsine, and C. W. Rose (1993), Modeling soil erosion by overland flow: Application over a range of hydraulic conditions, *Trans. ASAE*, *36*(6), 1743–1753.
Romkens, M. J. M., K. Helming, and S. N. Prasad (2001), Soil erosion under different rainfall intensities, surface roughness, and soil water regimes, *Catena*, *46*(2–3), 103–123.
Rose, C. W., J. R. Williams, G. C. Sander, and D. A. Barry (1983a), A mathematical model of soil erosion and deposition processes: II. Application to data from an arid-zone catchment, *Soil Sci. Soc. Am. J.*, *47*(5), 996–1000.
Rose, C. W., J. R. Williams, G. C. Sander, and D. A. Barry (1983b), A mathematical model of soil erosion and deposition processes: I. Theory for a plane land element, *Soil Sci. Soc. Am. J.*, *47*(5), 991–995.
Rose, C. W., B. Yu, H. Ghadiri, H. Asadi, J. Y. Parlange, W. L. Hogarth, and J. Hussein (2007), Dynamic erosion of soil in steady sheet flow, *J. Hydrol.*, *333*(2–4), 449–458.
Rudolph, A., K. Helming, and H. Diestel (1997), Effect of antecedent water content and rainfall regime on microrelief changes, *Soil Technol.*, *10*, 69–81.
Sander, G. C., P. B. Hairsine, C. W. Rose, D. Cassidy, J. Y. Parlange, W. L. Hogarth, and I. G. Lisle (1996), Unsteady soil erosion model, analytical solutions and comparison with experimental results, *J. Hydrol.*, *178*(1–4), 351–367.
Sander, G. C., P. B. Hairsine, L. Beuselinck, and G. Govers (2002), Steady state sediment transport through an area of net deposition: Multisize class solutions, *Water Resour. Res.*, *38*(6), 1087, doi:10.1029/2001WR000323.
Sander, G. C., T. Zheng, and C. W. Rose (2007a), Update to "Modeling water erosion due to overland flow using physical principles: 1. Sheet flow," *Water Resour. Res.*, *43*, W04408, doi:10.1029/2006WR005601.
Sander, G. C., J. Y. Parlange, D. A. Barry, M. B. Parlange, and W. L. Hogarth (2007b), Limitation of the transport capacity approach in sediment transport modeling, *Water Resour. Res.*, *43*, W02403, doi:10.1029/2006WR005177.
Sharmeen, S., and G. R. Willgoose (2006), The interaction between armouring and particle weathering for eroding landscapes, *Earth Surf. Processes Landforms*, *31*(10), 1195–1210.
Sharmeen, S., and G. R. Willgoose (2007), A one-dimensional model for simulating armouring and erosion on hillslopes: 2. Long term erosion and armouring predictions for two contrasting mine spoils, *Earth Surf. Processes Landforms*, *32*(10), 1437–1453.
Simon, A., and J. C. Collison (2001), Pore-water pressure effects on the detachment of cohesive streambeds: Seepage forces and matric suction, *Earth Surf. Processes Landforms*, *26*, 1421–1442.
Svoray, T., and S. Ben-Said (2010), Soil loss, water ponding and sediment deposition variations as a consequence of rainfall intensity and land use: A multi-criteria analysis, *Earth Surf. Processes Landforms*, *35*(2), 202–216.
Walker, J. D., M. T. Walter, J. Y. Parlange, C. W. Rose, H. Meerveld, B. Gao, and A. M. Cohen (2007), Reduced raindrop-impact driven soil erosion by infiltration, *J. Hydrol.*, *342*(3–4), 331–335.
Ward, P. J., R. T. v. Balen, G. Verstraeten, H. Renssen, and J. Vandenberghe (2009), The impact of land use and climate change on late Holocene and future suspended sediment yield of the Meuse catchment, *Geomorphology*, *103*(3), 389–400.
Willgoose, G. R., and S. Sharmeen (2006), A one-dimensional model for simulating armouring and erosion on hillslopes: 1. Model development and event-scale dynamics, *Earth Surf. Processes Landforms*, *31*(8), 970–991.
Woolhiser, D. A., R. E. Smith, and D. C. Goodrich (1990), KINEROS, A kinematic runoff and erosion model: Documentation and user manual, *Rep. ARS-77*, p. 130, Agric. Res. Serv., U.S. Dep. of Agric., Washington, D. C.
Wuddivira, M. N., R. J. Stone, and E. I. Ekwue (2009), Clay, organic matter, and wetting effects on splash detachment and aggregate breakdown under intense rainfall, *Soil Sci. Soc. Am. J.*, *73*, 226–232.